Journal of Computational Applied Mechanics 2021, 52(3): 717-730
DOI: 10.22059/jcamech.2021.332426.656

RESEARCH PAPER

Modeling and Optimizing Creep behavior of A356 Al Alloy in Presence of Nickel Using Response Surface Method.

Mohammad Varmazyar[1], Shahrouz Yousefzadeh[1,*], Sheikhi Mohammad Morad[1,2]
[1]*Department of Mechanical Engineering, Aligudarz branch, Islamic Azad University, Aligudarz 6861885914, Iran*
[2]*Faculty of Mechanical Engineering, Shahid Rajaee Teacher Training University, Tehran 1678815811, Iran*

Abstract

The present paper aims to model the creep behavior of A356 Al alloy in the presence of different amounts of nickel and evaluate the microstructure of the alloys using optical microscope and scanning electron microscope (SEM). Creep properties of the alloys were obtained using the impression creep method by a cylindrical indenter within the stress range of $0.027<\sigma/G<0.030$ at 473-513K. As indicated by the results, adding nickel to A356 alloy would result in eliminating the harmful phases of iron, modifying the morphology of α-Al dendrites, and creating new nickel-rich phases, besides improving the creep strength of the alloy. This is due to the formation of nickel-rich intermetallic compounds and prevention from the formation of iron-rich phases. By calculating the creep activation energy and stress power, it was found that the climb-controlled dislocation creep in the dominant mechanism network in the creep deformation of A356 alloy was in the cast state and under the studied conditions. Also, nickel had no effect on the creep mechanism. Besides, the equation of the creep deformation of the alloys (the relationship between temperature, stress, and stable-state creep strain rate) was obtained. This equation can be used to predict the stable-state creep strain rate at certain temperature and stress for A356 alloy and nickel-containing alloys under climb controlled dislocation creep conditions.

Keywords: Optimization, A356 alloy, Nickel, Microstructure, Impression creep, Creep mechanism, Response surface

1. Introduction

Design of experiment (DoE) refers to a set of actions performed by modeling and optimizing the reaction variables through statistical methods in order to increase the efficiency without increasing the price. In traditional DoE methods, only one factor is assumed as the variable and other factors are considered at a constant level. Such a method is called one-variable-at-a-time technique, in which the mutual effects of the variables are not studied and complete effects of the factors in the procedure cannot be demonstrated. Moreover, conducting the research requires several experiments, which resulted in the increase in time, cost, and consumption of materials and reagent. To overcome this problem, the RSM method was presented for optimization studies by Box and Wilson, which was later developed by engineers and scientists. In general, the optimization studies by RSM method can be divided into the following five stages:

1) Selecting the variables that are independent of the major effects on the system through screening and restricting the experiment region limits with regard to the research objectives and researcher experience;

2) Selecting the experiment design and performing the experiments with regard to the selected experimental field;

* Corresponding author: shahrouzyousefzadeh@gmail.com

3) Evaluating the model's proportion;

4) Approving the necessity and possibility of displacement along the direction of the desired region; and

5) Obtaining the optimal values for each of the studied variables [1];

Generally, advantages such as low density, high strength-to-weight ratio, excellent casting capability, high electrical and thermal conduction, good machining capability, and excellent resistance against corrosion can be assumed for aluminum and its alloys [2]. Among the commercial cast Al alloys, the alloys that contain silicon as the main alloy element are widely used due to their excellent casting characteristics. Adding silicon to aluminum results in high fluidity, good feeding, low contraction, and hot crack-resistance, so that more than 90% of the cast Al alloys fall in this category [3], causing the wide use of these alloys in various fields including automotive manufacturing, aerospace, as well as defense and military industries. The strength-to-weight ratio is one of the interesting characteristics of these alloys. Density of aluminum is 2.7gr/cm3, which is nearly one-third of steel, copper, and brass. Yet, silicon with the density of 2.3gr/cm3 is an element, the addition of which to aluminum does not reduce the advantage of low weight of aluminum [4]. A356 alloy is a hypoeutectic alloy of the aluminum-silicon alloy system,

which is widely used in automotive and aerospace industries due to its properties such as excellent casting capability, low contraction, excellent strength-to-weight ratio, good corrosion-resistance, and excellent abrasion-resistance [5]. Impression creep includes the movement of the voids under the applied stress throughout the crystal. This mechanism occurs usually at low stress levels. Movement of the voids and interstitial atoms through penetration in the network or grain boundaries results in the creep of the poly-crystal. Each of these two streams (flow) paths contributes to the strain rate independently [6]. Also, movement of the dislocations causes plastic deformation of the material. Exposure of dislocations to obstacles such as the grain boundary sediments and other dislocations results in the increased strength of the material at low temperatures. At high temperatures, dislocations can pass these obstacles. In addition to cross sliding as one of the ways for escaping the obstacles, climbing of the dislocations, which is a penetration process, is considered the main mechanism for passing the obstacles. In fact, in this creep mechanism, movement of the dislocations occurs due to the heat-activated processes such as the penetration of voids and interstitial atoms. Therefore, the creep rate not only depends on temperature and stress, but also is a function of other characteristics of the material such as penetration coefficient and stacking-fault energy. Once the climbing process occurs due to the application of relatively high stresses, the dislocations inside the poly-crystal grains start to move and aggregation of these grains results in forming the dislocation cells inside the grain [7]. Moreover, in grain boundary sliding, if the applied stress is enough (i.e., above the threshold level), then, the velocity of the grain boundary sliding-caused strain will be even higher than other velocities of the creep mechanism. As indicated by the results, the velocity of the grain boundary sliding-caused creep can be up to ten times more than that of the impression creep [8].

In the few past decades, the impression creep experiment method has attracted the attention of many researchers. In the studies conducted in this field, researchers have used various types of the indenters including pyramidal, spherical, and conic indenters and have proposed several equations for finding the creep rate proportionate to the applied conditions [9].

Creep in mono-crystals occurs due to the dislocation processes because due to the lack of grain boundaries, penetration mechanisms have an insignificant contribution to the overall creep rate. Thus, the Harper-Dorn creep can be one of the dislocation creep processes in coarse-grained

aluminum near the melting point [10]. In [11], the authors investigated the effect of deformation in equal-channel angular pressing (ECAP) on the creep of pure aluminum within the stress range of 10-50MPa at 473K. They showed the creep mechanism was indeed the sliding and climbing of the dislocations and, due to the instability of the super fine-grained structure at 473K, the impression creep was unstable and growth of the grains prevented Coble impression creep. Moreover, Sedaico et al. (2016) studied the creep behavior of silicon-containing aluminum within the temperature range of 200-2500C and stress range of 45-100MPa using in-situ neutron diffraction method. According to their results, creep of dislocations was the dominant mechanism at low stress values, which was converted into power law breakdown (PLB) by increasing the stress value. In [12], the authors added different amounts of copper to Al-17Si-0.5Mg alloy in order to investigate the microstructure and impression creep behavior of the alloy. Adding copper to the alloy resulted in modifying the microstructure and eutectic of silicon and, thereby, improving the alloy's creep behavior. The increase in the creep strength was due to the presence of copper-rich phases with high thermal stability, which prevented grain boundary sliding. Moreover, copper reduced the stacking-fault energy by being dissolved in aluminum. According to the report in [13], adding scandium to Al-Si alloy caused modifying the microstructure and improving the behavior of the alloy at high temperatures. Improvement of the creep properties was attributed to modifying the microstructure and the scandium-rich sediments, which caused pinning of the grain boundaries. In [14], the authors added slight amounts of Mn, Ti, and V and the considerable amount of Cu to Al7SiMg alloy in order to investigate its behavior at high temperatures. The presence of these elements in the alloy increased the hot tensile strength and creep properties of the alloy, so that the tensile strength of this alloy was significantly higher than the base alloys within the range of 250-3000C, which introduced it as a good choice for cylinder heal parts. In [15], the authors investigated the simultaneous effects of zirconium and vanadium on the mechanical properties of AlSi9Cu2 cylinder head alloy. Casting this alloy was performed using tilt casting method in order to prevent turbulence and chaos. Adding zirconium and vanadium caused the alloy's microstructure be converted from a coaxial dendritic structure into a coaxial micro-column microstructure. Studying the simultaneous effects of zirconium and vanadium on A356 alloy's microstructure showed adding these two elements at the same time had a more effect on the modification of the grains. Comparing gadolinium, strontium, and zirconium separately as the eutectic silicon modifier showed that adding zirconium and gadolinium at the same time resulted in forming numerous nano-sediments on the eutectic silicon, which prevented their growth during solidification and could be an excellent modifier for eutectic silicon [16].

In [17], by adding different amounts of nickel and molybdenum to Al-7Si alloy, the authors found these elements could improve mechanical properties of this alloy at nearly 2300C and modify the alloy's microstructure by forming thermally stable phases. It was reported that, in the case of adding some nickel to A319 alloy and applying thermal treatment of it, nickel would result in forming the nickel-rich intermetallics and, thereby, directly affect the alloy's microstructure and hardness improvement. As indicated by microstructural studies using TEM method, nickel affects the morphology, distribution, and mainly type, size, and amount of the sediments formed during the aging process [1]. In [18], by adding 1% nickel to Al-12Si alloy, the researchers found the presence of nickel resulted in the eutectic modification of silicon, improvement of strength at 350oC, and resistance against the alloy's creep. Such a behavior resulted from the presence of the nickel-rich intermetallics. As reported in [19], the nickel-rich compounds had good thermal stability in Al-Si alloys and led to the improved creep properties of these alloys. Also, in [20], the authors investigated the simultaneous effect of graphite, copper, and nickel on Al-Si alloy's microstructure and found the simultaneous addition of these elements would have more

effect on the reduction of the grain size and improvement of the alloy's strength at high temperatures. Al-Si alloy's ductility and strength were improved by adding graphite, copper, and nickel at the same time. The fractographic examinations of the alloy showed that by increasing the temperature during the tensile test (tension test), the fracture model was converted from brittle fractures at the ambient temperature into soft fractures at high temperatures. In addition, in [21], the researchers investigated the strengthening effect of the heat-resistant phases on the Al-Si piston alloy with different Fe/Ni ratios. According to the results, with an increase in the Fe/Ni ratio, the heat-resistant phases were formed, which subsequently resulted in improving the morphology and distribution in the alloy.

Although many studies have been conducted on the high-temperature behavior of Al-Si alloys, there are only a few WORKS on modeling and optimizing the effect of different amounts of nickel on the microstructure and creep behavior of these alloys. Hence, the present work is focused on A356 alloy casting using tilt casting method.

2. Principles of DoE of creep rate by RSM

Design of the experiment of the RSM arrangement by DOE method and the number of required experiments are presented in Table (1). (Figure 1) shows the graphic design of the structure and casting of the above-mentioned alloys as well as different stages of the applied experiments in order for examining the alloy's microstructure. Moreover, Figure (2) shows different stages of preparing the creep experiment samples as well as conditions of the experiment.

Table 1: Design of experiment by RSM

RUN	Factor 1	Factor 2	Factor 3
	A: Temperature (°C)	B: Stress (MPa)	C: Alloy
1	240	600	A356+0.25Ni
2	200	600	A356+1Ni
3	220	625	A356+0.25Ni
4	240	650	A356+0.25Ni
5	240	600	A356
6	220	675	A356
7	200	600	A356+0.25Ni
8	240	675	A356+0.25Ni
9	200	600	A356+0.5Ni
10	200	625	A356
11	220	625	A356+0.5Ni
12	240	625	A356+0.5Ni
13	200	625	A356+0.5Ni
14	220	600	A356
15	220	650	A356+1Ni
16	200	625	A356+1Ni
17	240	625	A356+0.25Ni
18	200	600	A356
19	220	675	A356+0.5Ni
20	240	600	A356+0.5Ni
21	200	650	A356+0.25Ni
22	220	625	A356+1Ni
23	200	675	A356
24	240	675	A356+1Ni

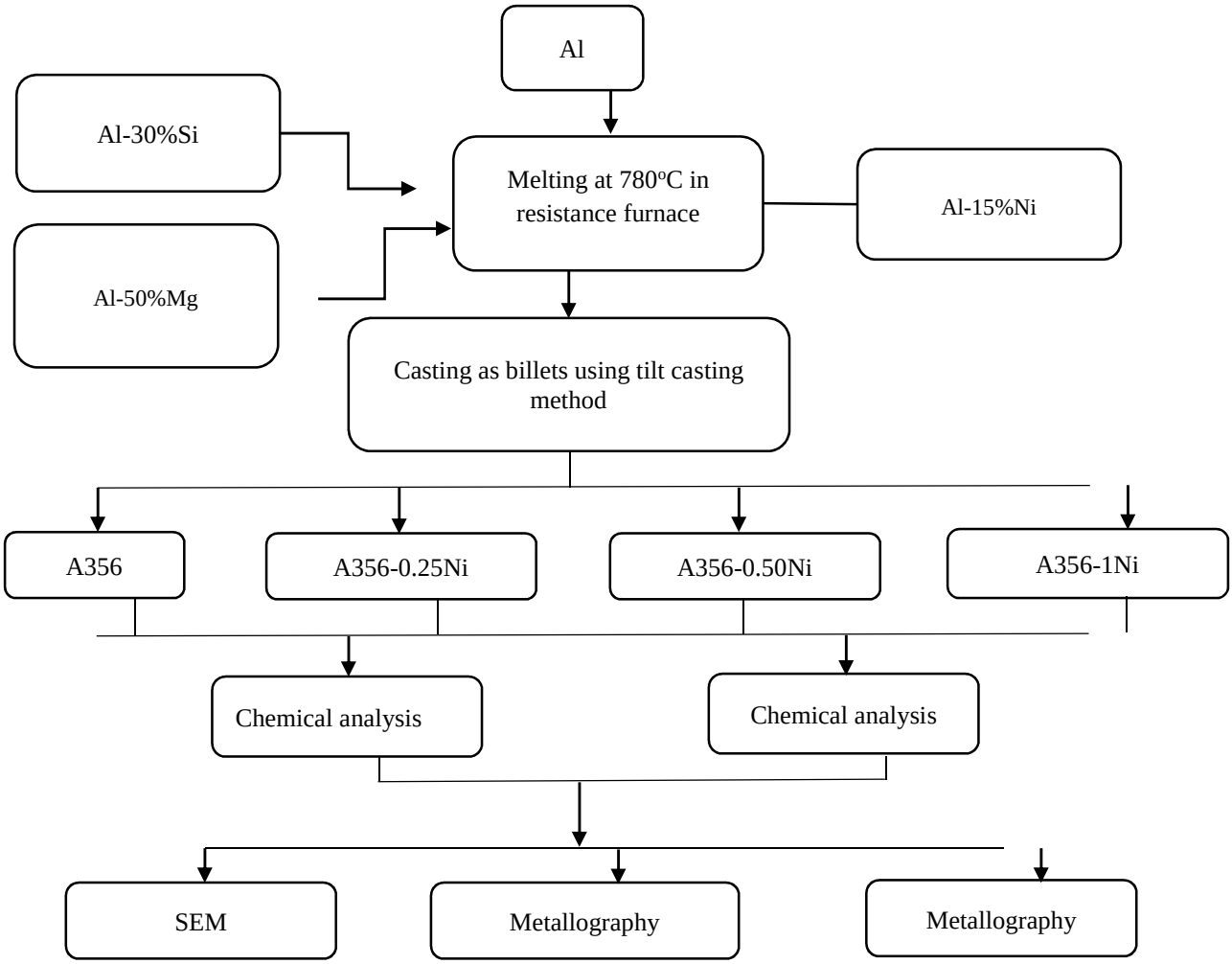

Figure1: Graphic design of the stages of construction and casting of the alloys used in the present study

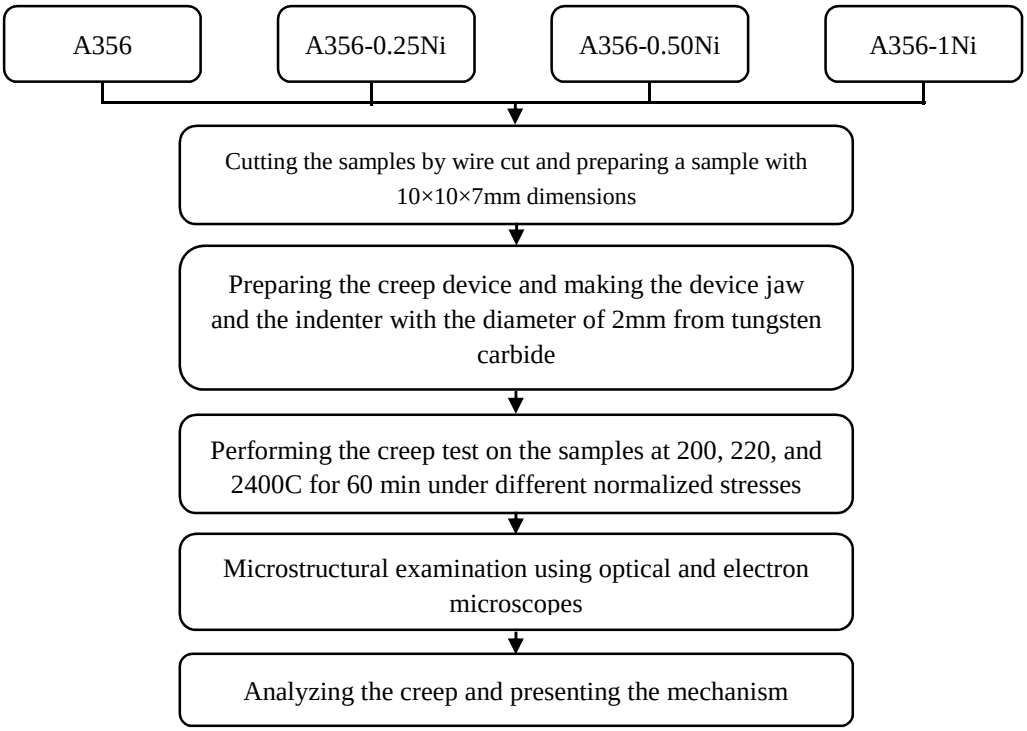

Figur 2: Graphic design of the preparation stages of the samples for creep experiment

3. A356 alloy

In the proposed model, pure aluminum (99.92%), Al-50%Mg hardener (master alloy), and Al-30%Si were used for producing A356 alloy with (Al-7Si-0.3Mg) nominal combination. The alloy was melted in an electrical resistance furnace. First, the furnace was preheated up to 250oC. Once aluminum was melted at 7300C in a graphite crucible; first, the Al-30%Si hardener and, then, the Al-50%Mg hardener were added to melted material. Also, the melting loss was taken into consideration in order to ensure the chemical combination of the alloy. To make sure the homogeneity, the melted compound was stirred by a graphite electrode for 2 min. After degassing by C2Cl6 pills (0.3 wt%) for 2 min and separating the slag, the compound was casted as billets in a cast iron mold, which was preheated to 2000C and connected to a tilt casting system. Figure (3) shows the tilt molten pouring system.

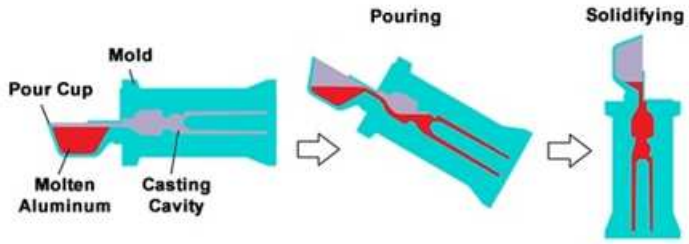

Figure 3. Schematic view of tilt casting system

4. Nickel-containing alloys

To prepare the nickel-containing alloys, just like A356 alloy, after melting the aluminum at 720^{o}C and adding silicon and magnesium hardeners, the temperature increased up to 780^{0}C and, then, Al-

15%Ni hardener with certain weight percentage was added to the molten material. Then, using a graphite electrode, the compound was stirred mechanically; after 10 min and isolating the slag, just like A356 alloy, the molten compound was casted as billets in a cast iron mold, which was preheated to 200^0C and connected to the tilt casting system.

5. Preparing the creep samples

In the present work, the creep experiment was performed on the casting samples according to the introduced graphic design. First, the samples with 10×10×7mm dimensions were cut from casted billets using a wire cut. Then, the two surfaces of the samples were machined using sandpapers 100-1500. Moreover, once the samples were prepared, the parallelism of the two surfaces was checked by a caliper in all the sections. Figure (4) shows a schematic view of the casting and creep sample.

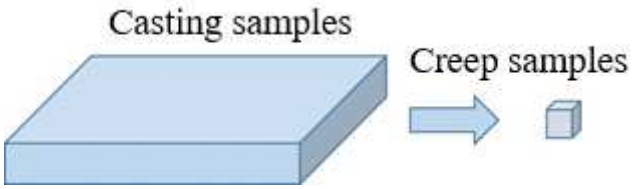

Figure 4: Schematic view of the casting and creep sample

6. Impression creep apparatus

Performing the creep experiments required an impression creep apparatus with a cylindrical indenter with the dimension of 2mm made from tungsten carbide. For this purpose, the Universal hot tension test apparatus, model STM-50, with the capacity of 5 ton manufactured by SANTAM CO was used. This apparatus is shown in Figure (5).

Figure 5: Creep apparatus used in the present study

7. Experiment method

In the creep experiment, regarding the large dimensions of the apparatus, in order to eliminate the length changes resulting from the thermal expansion and thermal equilibrium, the apparatus was switched on 2 h before starting the experiment. Then, the prepared samples were put in the apparatus. Also, after 20 min, the intended load was applied in order to obtain the isothermal sample. After applying the load, variations of the indenter's depth were recorded completely by the software. The creep experiment was performed on the samples at 200, 220, and 240^0C and stress-to-shear modulus ratios of 0.027, 0.028, 0.029, and 0.03 (σ/G) for 60 min.

8. Hardness assessment

Hardness of the studied alloys was determined using a hardness tester apparatus, model Buehler MXT-al, with the load of 500kf and ball diameter of 10mm (balls were made of hardened steel).

9. Simulation results

Figure (6) shows the optical microstructure of A356 alloy in two different magnification degrees. As mentioned in the literature review, regarding the dual Al-Si graph, the eutectic changes occurred in the 12wt% chemical combination of silicon. Since A356 alloy contained nearly 7% silicon, the first phase would coincide the solidification of α-Al. Also, after completing the solidification at the eutectic temperature, A356 alloy's microstructure would contain coarse dendritic initial α-Al and a eutectic α-Al+Si mixture, so that silicon would have coarse and dish-shaped eutectic morphology.

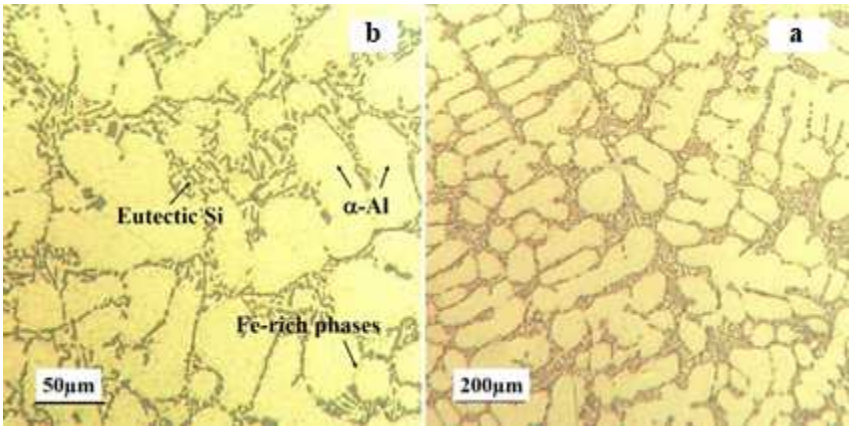

Figure 6: Microstructure of A356 alloy under an optical microscope with two different magnifications

In order for more precise identification of the phases, the electron microscope image of these alloys along with the point analysis spectrum of the phases is shown in Figure (7). According to Figures (7-a) and (7-b), adding 0.25% nickel resulted in the formation of an iron- and nickel-rich intermetallic compound, which was named as AlSiNiFe due to the lack of good reference in this regard and failure to detect this phase in the XRD spectrum. This intermetallic compound had block-shaped morphology and was formed in the eutectic region and in the common area of silicon eutectics and α-Al dendrites. As shown in Figure (7), by increasing the nickel content from 0.25wt% to 1wt%, the morphology of these phases gradually changed, so that it was converted from block-shaped morphology into needle-shaped morphology. Besides, the formation place of the needle-shaped AlSiNiFe compound was on the silicon eutectics, the value of which increased by increasing the amount of nickel. The volumetric fraction of the intermetallics for A356, A356-

0.25Ni, A356-0.5Ni, A356-1Ni was obtained equal to 0.22%, 1.35%, 2.89%, and 4.1%, respectively.

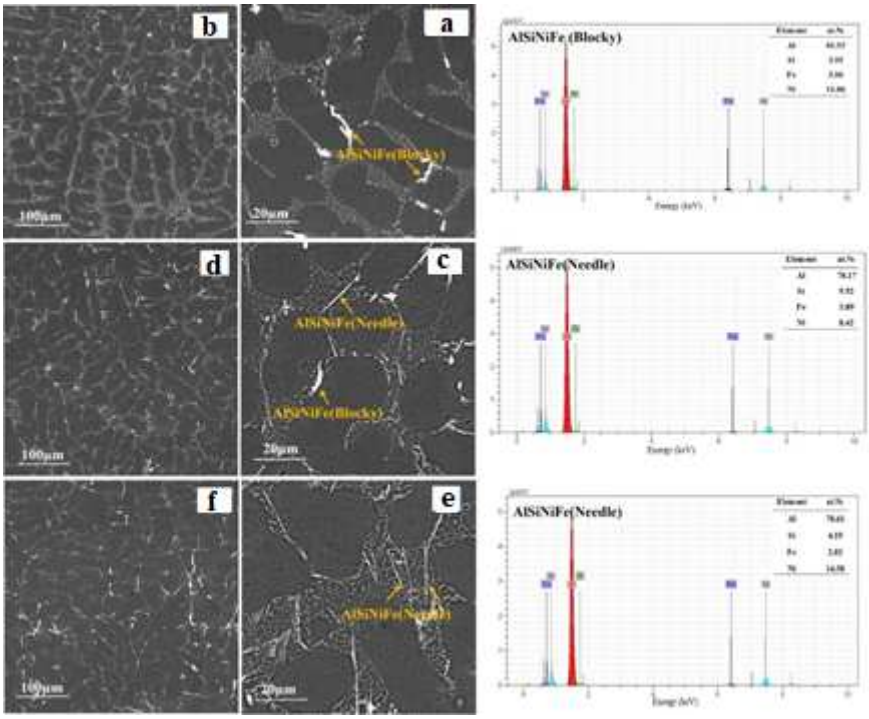

Figure 7: BSE microstructure of the alloys: a) A356-0.25; b) A456-0.5Ni; c) A356-1Ni along with the EDX spectrum of the phases

Figure (8) shows the creep diagram of A356, A356+0.25Ni, A356+0.5Ni, and A356+1Ni alloys at 513K and under normalized stress of (σ/G)=0.029 for 3600s. Since the shear modulus was constant, instead of applying a constant stress at different temperatures, constant normalized stress (σ/G) was applied. In this equation, σ is the applied stress and G is the shear modulus for aluminum, which can be obtained as a function of temperature from the following equation [22]:

$$G\ (MPa)=30000-18T\ (K) \quad (1)$$

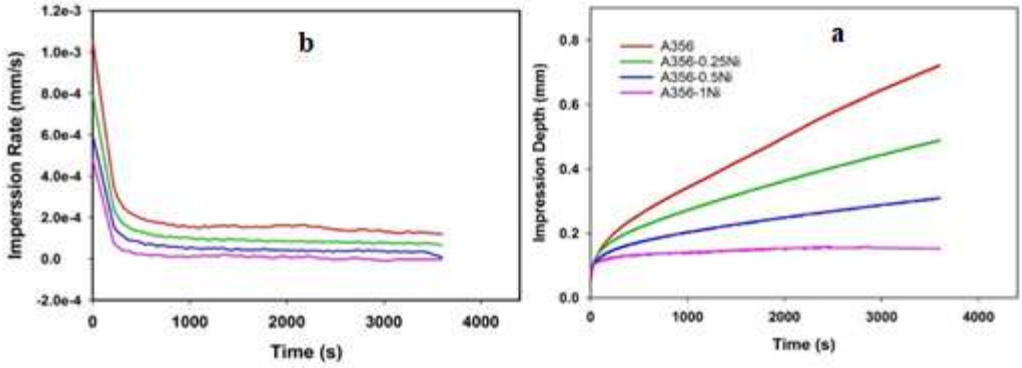

Figure 8: Indenter's depth variations in terms of time at 513 K under normalized stress of (σ/G)=0.029: a) variations of penetration depth versus creep time; b) variations of creep rate versus creep time

It is observed that for all the alloys, the creep curve consisted of two primary creep and secondary creep regions. The third phase in these curves was not observed due to the compressive

nature of the experiment and the application of constant stress. According to Figure (8-b), in these curves, first, speed of the indenter's variations was reduced over time and gradually became constant as time passes, which indicated the secondary creep. Since the temperature of the experiments in this study was above the recrystallization temperature of the aluminum alloy [23], it was possible to retrieve the dislocations during the creep. Accordingly, the reduction in the strain rate indicated the dominance of the work hardening process over the retrieval, while the point that the strain rate became constant over time implied the beginning of the stable-creep region and the hard work hardening-retrieval balance.

Figure (9) shows the stable-state creep rate of the alloys at different temperatures and stresses. According to the results, the creep properties of A356 alloy were improved by adding nickel, so that 356-1Ni alloy exhibited highest creep strength.

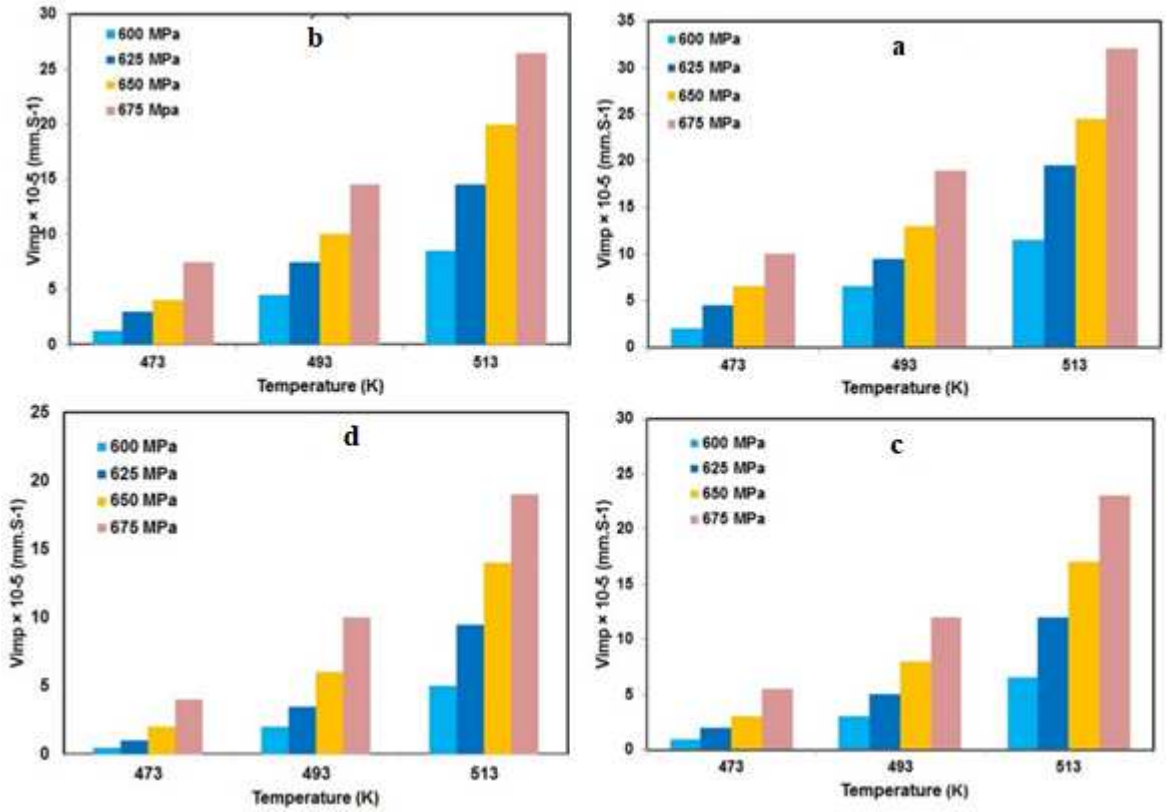

Figure 9: Comparing impression creep velocity variations at different temperatures under different stresses: a) A356; b) A356-0.25Ni; c) A356-0.5Ni; d) A356-1Ni

Figure (10) shows the variations of $lnV_{imp}T/G$ in terms of l/T under constant normalized stresses for all alloys, which were obtained using the creep activation energy lines gradient. The activation energy value varied between 122 and 155kJ/mol, and the average activation energy for A356, A356-0.25Ni, A356-0.5Ni, A356-1Ni alloys was 137±7.2, 5.6±1, 141.7±5.139, and 145.3±4.3 Kj/mol, respectively. As reported, the activation energy for penetration into the dislocation channel and penetration into the network for aluminum was 82 and 143 Kj/mol, respectively. The activation energy for all the alloys was close to the penetration into the network. Thus, by comparing the obtained results, it can be concluded that the creep of all alloys was caused by the creep of dislocations and the dominant mechanism in controlling the creep velocity of the alloys would be the climb-controlled dislocation through penetration into the network.

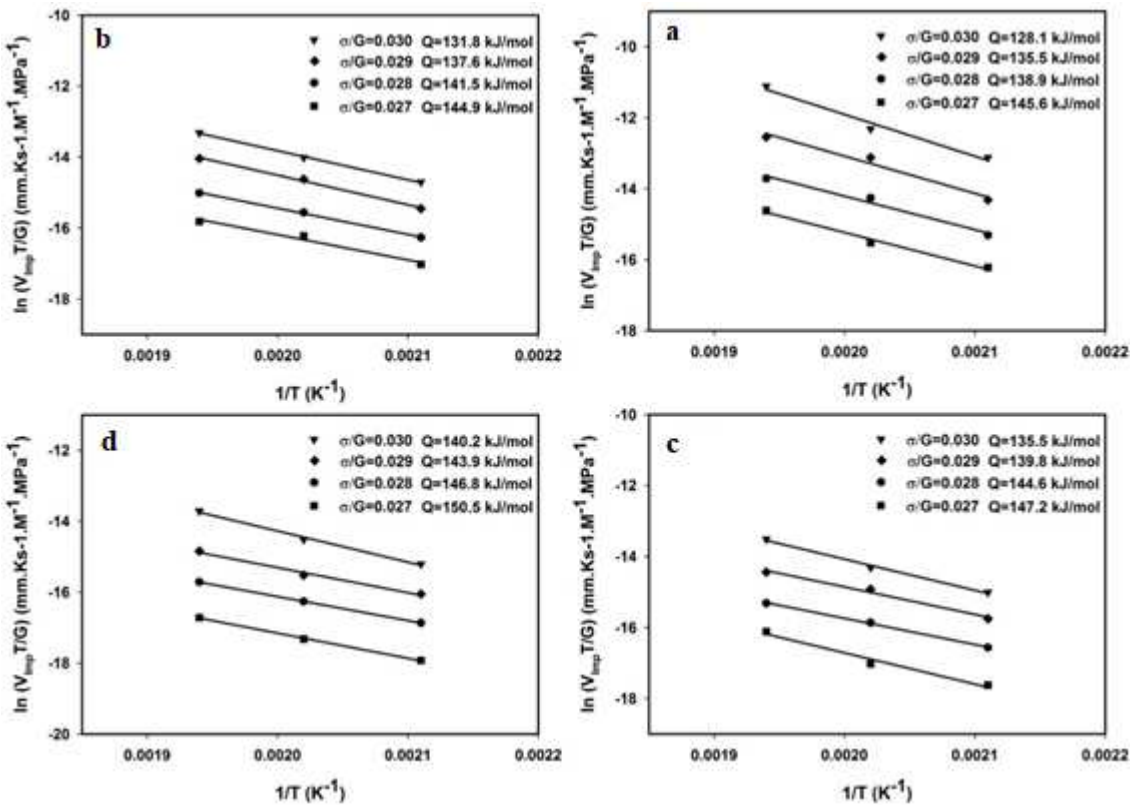

Figure 10: Variations of $\boldsymbol{ln}\left(\frac{V_{imp}T}{G}\right)$ in terms of 1/T under constant normalized stress for determining the activation energy of all alloys

Figure (11) shows the BSE image of all the alloys after creeping under the indenter at 493K under the stress of (σ/G) =0.029. In A356 alloy, it is observed that in the second region, the ground phase was considerably deformed along the shear stress, so that the silicon blades were broken into small pieces and lost their continuousness eutectic phase. Besides, this β phase was broken into small pieces along the direction of the deformation, indicating the low strength of this phase under the experiment conditions.

Moreover, in nickel-containing alloys (Figure 11-b to 11-d), by increasing the nickel content, the eutectic phase was kept constant and the deformation was reduced. Also, in the nickel-containing alloys and in the deformation region, AlSiNiFe intermetallic compounds were not deformed, especially in A356-1Ni alloy, and the amount of these intermetallic compounds increased in the deformation region with an increase in the nickel content.

The diagram of creep rate under different conditions for the alloy in Figure (12) shows the effect of nickel at different stresses.

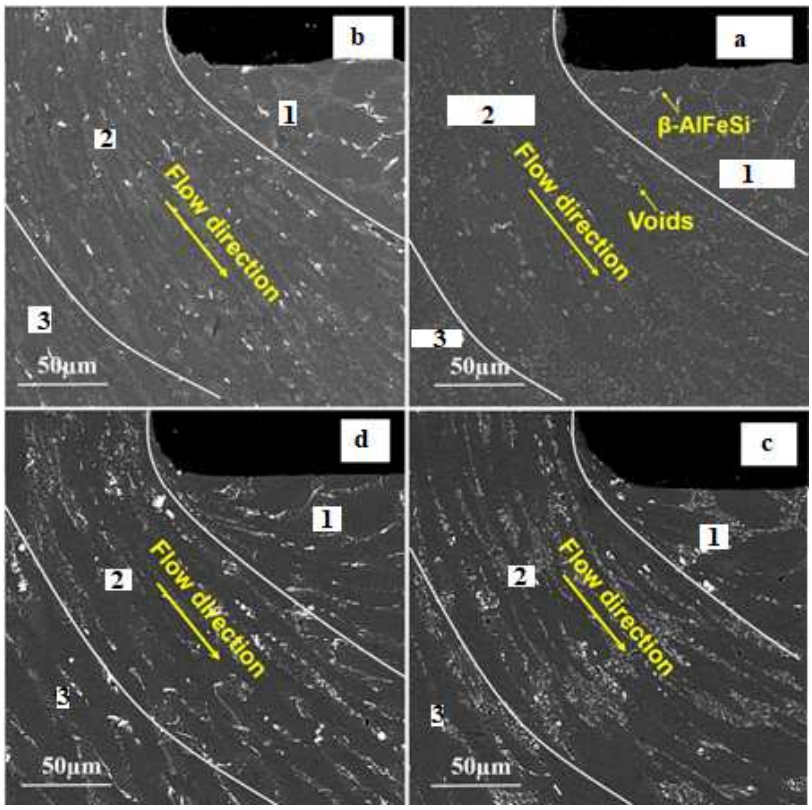

Figure 11: BSE image of the microstructure after creeping at 493K under stress of (σ/G)=0.029 for 3600s: a) A356; b)A356-0.25Ni; c) A356-0.5Ni, d) A356-1Ni

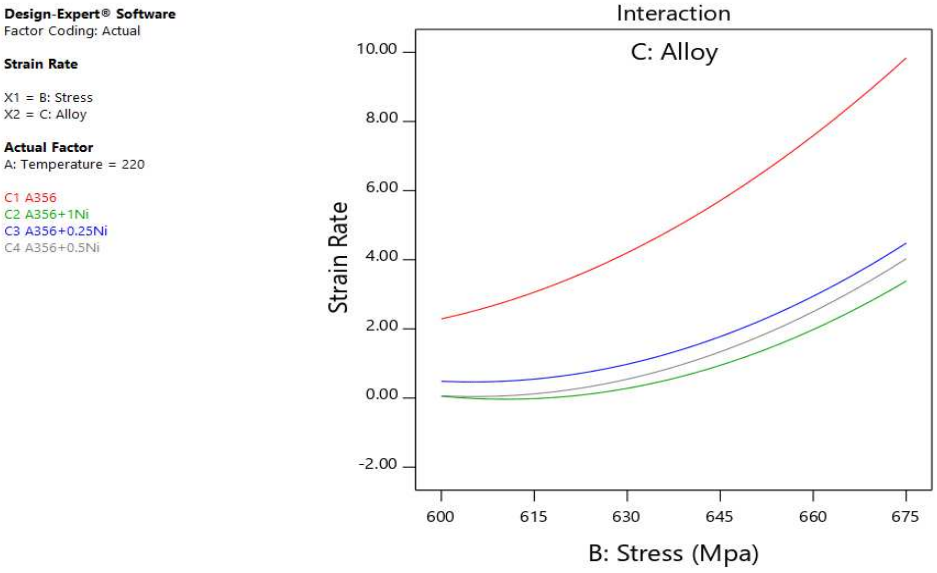

Figure-12: Diagram of creep rate under different average conditions of the alloy using RSM method

In the above diagram, the red line, which represents the base A356 alloy, incurred the highest creep rate. Next to it is the blue line where the creep rate is reduced by adding 25% nickel to the base alloy. As for the gray line, adding 0.5% nickel to the base alloy leads to a reduction in the creep rate. And finally, the green line represents the lowest creep rate which is obtained by adding 1% nickel to the base alloy.

Figure (13) represents the 2D interaction of two quantitative variables, namely temperature and stress, on the creep rate, so that the blue region indicates the lowest creep rate in the most optimal range of 1% nickel.

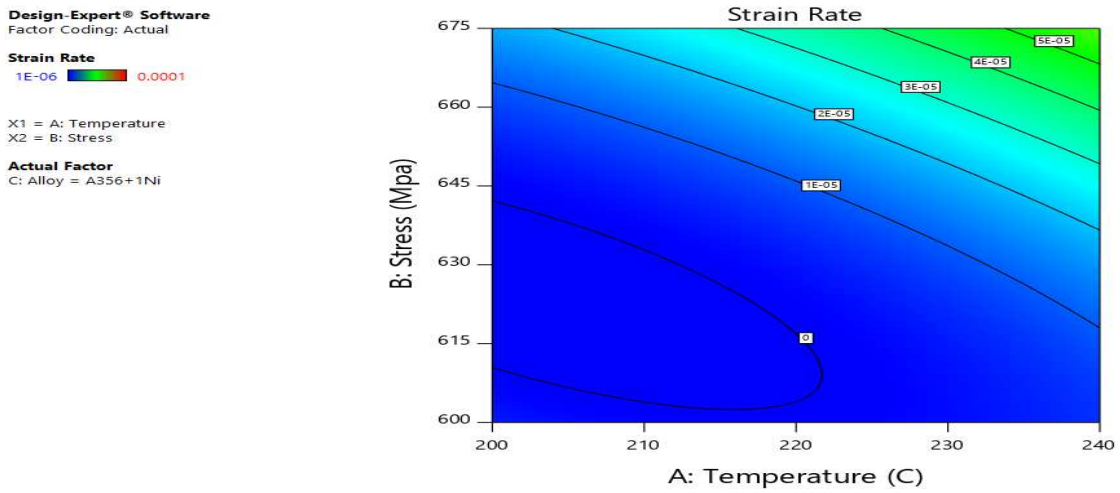

Figure 13: 2D diagram of the effect of 1% nickel in the most optimal state using RSM method

10. Conclusion

In the present study, the effect of different nickel contents on the creep behavior of A356 aluminum alloy as well as the performance of the microstructures was investigated macroscopically using the flat-ended cylindrical impression creep mechanism. The experiment was performed within the temperature range of 493-513K and stress range of 600-675MPa in the casting mode. Then, the experimental values were put in the optimizer software environment, so that besides approving the experimental work of investigating the effect of nickel, the best creep rate was obtained. The microstructure of A356 alloy included α-Al dendrites with the coarse and column-shaped morphology, silicon eutectics, and iron-rich β-AlFeSi intermetallic compounds. Also, adding nickel to A356 alloy resulted in the reduced grain size, reduced α-Al dendrite size, and modified silicon eutectic morphology. Moreover, adding nickel to A356 alloy improved the creep strength of the alloy, so that A356-1Ni alloy exhibited the highest creep strength, which was due to the formation of the nickel-rich intermetallic compounds in the inter-dendrite regions, prevention of the formation of iron-rich compounds, and modification of the silicon eutectic morphology.

The stress power values for the creep of the studied alloys indicated the creep of the climb controlled dislocations. Also, the activation energy values for the creep of different alloys implied the control of the dislocation climbing velocity through penetration into the network. Moreover, the creep deformation equation could be used to determine the secondary creep strain rate at the climb controlled dislocation creep.

Based on the RSM method, the most optimal state of the effect of nickel on the creep rate in this experiment was in the 1%-nickel state at 204^0C and under the stress of 607.5MPa. Also, in the proposed experiment, the effect of the value of the input stress parameter on the creep rate was more than that of temperature.

11. References

[1] R. H. Myers, D. C. Montgomery, C. M. Anderson-Cook, 2016, *Response Surface Methodology: Process and Product Optimization Using Designed Experiments*, Wiley,

[2] S. K. Mishra, H. Roy, A. Mondal, K. Dutta, Damage assessment of A356 Al alloy under ratcheting–creep interaction, *Metallurgical and Materials Transactions A*, Vol. 48, No. 6, pp. 2877-2885, 2017.

[3] M. Reihanian, K. Ranjbar, S. Rashno, Microstructure and impression creep behavior of Al–7Si–0.3 Mg alloy with Zr addition, *Metals and Materials International*, Vol. 27, No. 8, pp. 2530-2540, 2021.

[4] S. M. Miresmaeili, B. Nami, R. Abbasi, I. Khoubrou, Effect of Cu on the creep behavior of cast Al-15Si-0.5 Mg alloy, *JOM*, Vol. 71, No. 6, pp. 2128-2135, 2019.

[5] R. Long, E. Boettcher, D. Crawford, Current and future uses of aluminum in the automotive industry, *JOM*, Vol. 69, No. 12, pp. 2635-2639, 2017.

[6] L. Zuo, B. Ye, J. Feng, X. Kong, H. Jiang, W. Ding, Microstructure, tensile properties and creep behavior of Al-12Si-3.5 Cu-2Ni-0.8 Mg alloy produced by different casting technologies, *Journal of materials science & technology*, Vol. 34, No. 7, pp. 1222-1228, 2018.

[7] S. Roy, L. F. Allard Jr, A. Rodriguez, T. R. Watkins, A. Shyam, Comparative evaluation of cast aluminum alloys for automotive cylinder heads: Part I Microstructure evolution, *Metallurgical and Materials Transactions. A, Physical Metallurgy and Materials Science*, Vol. 48, No. 5, 2017.

[8] D. G. Sediako, W. Kasprzak, F. Czerwinski, A. M. Nabawy, A. R. Farkoosh, *High temperature creep evolution in Al-Si alloys developed for automotive powertrain applications: a neutron in-situ study on Hkl-plane creep response*, in: *Light Metals 2016*, Eds., pp. 131-136: Springer, 2016.

[9] P. Seensattayawong, P. Pandee, C. Limmaneevichitr, Impression creep properties of hypoeutectic Al-Si alloys with scandium additions, *Materials Today: Proceedings*, Vol. 5, No. 3, pp. 9440-9446, 2018.

[10] W. Liu, W. Xiao, C. Xu, M. Liu, C. Ma, Synergistic effects of Gd and Zr on grain refinement and eutectic Si modification of Al-Si cast alloy, *Materials Science and Engineering: A*, Vol. 693, pp. 93-100, 2017.

[11] E. Kilinc, N. Kiremitci, Y. Birol, E. Dokumaci, Effect of Vanadium and Zirconium Additions on Mechanical Properties and Microstructure of Gravity Die-Cast AlSi9Cu2 Alloy Cylinder Heads, *International Journal of Metalcasting*, Vol. 13, No. 1, pp. 137-145, 2019.

[12] F. Meng, Y. Wu, K. Hu, Y. Li, Q. Sun, X. Liu, Evolution and strengthening effects of the heat-resistant phases in Al–Si Piston alloys with different Fe/Ni ratios, *Materials*, Vol. 12, No. 16, pp. 2506, 2019.

[13] T. Bogdanoff, A. K. Dahle, S. Seifeddine, Effect of Co and Ni addition on the microstructure and mechanical properties at room and elevated temperature of an Al–7% Si Alloy, *International Journal of metalcasting*, Vol. 12, No. 3, pp. 434-440, 2018.

[14] C. Xu, F. Wang, H. Mudassar, C. Wang, S. Hanada, W. Xiao, C. Ma, Effect of Sc and Sr on the eutectic Si morphology and tensile properties of Al-Si-Mg alloy, *Journal of Materials Engineering and Performance*, Vol. 26, No. 4, pp. 1605-1613, 2017.

[15] H. Medrano-Prieto, C. Garay-Reyes, C. Gómez-Esparza, I. Estrada-Guel, J. Aguilar-Santillan, M. Maldonado-Orozco, R. Martínez-Sánchez, Effect of Nickel addition and solution treatment time on microstructure and hardness of Al-Si-Cu aged alloys, *Materials Characterization*, Vol. 120, pp. 168-174, 2016.

[16] W. Prukkanon, N. Srisukhumbowornchai, C. Limmaneevichitr, Modification of hypoeutectic Al–Si alloys with scandium, *Journal of Alloys and Compounds*, Vol. 477, No. 1-2, pp. 454-460, 2009.

[17] G. Rajaram, S. Kumaran, T. S. Rao, Effect of graphite and transition elements (Cu, Ni) on high temperature tensile behaviour of Al–Si Alloys, *Materials Chemistry and Physics*, Vol. 128, No. 1-2, pp. 62-69, 2011.

[18] A. Farkoosh, X. G. Chen, M. Pekguleryuz, Dispersoid strengthening of a high temperature Al–Si–Cu–Mg alloy via Mo addition, *Materials Science and Engineering: A*, Vol. 620, pp. 181-189, 2015.

[19] M. Garat, Optimization of an aluminum cylinder head alloy of the AlSi7Cu3MnMg type reinforced by additions of peritectic elements, *International Journal of Metalcasting*, Vol. 5, No. 3, pp. 17-24, 2011.

[20] F. Kabirian, R. Mahmudi, Impression creep behavior of a cast AZ91 magnesium alloy, *Metallurgical and Materials Transactions A*, Vol. 40, No. 1, pp. 116-127, 2009.

[21] S. Miresmaeili, B. Nami, Impression creep behavior of Al–1.9% Ni–1.6% Mn–1% Mg alloy, *Materials & Design (1980-2015)*, Vol. 56, pp. 286-290, 2014.

[22] M. Yousefi, M. Dehnavi, S. Miresmaeili, Microstructure and impression creep characteristics Al-9Si-xCu aluminum alloys, *Metallurgical and Materials Engineering*, Vol. 21, No. 2, pp. 115-126, 2015.

[23] B. A. Esgandari, B. Nami, M. Shahmiri, A. Abedi, Effect of Mg and semi solid processing on microstructure and impression creep properties of A356 alloy, *Transactions of Nonferrous Metals Society of China*, Vol. 23, No. 9, pp. 2518-2523, 2013.